Reprinted from
PHILOSOPHICAL MAGAZINE, Vol. 14, No. 130, p. 689, October 1966

The Nature of Deformation Around Pressure Cracks on Diamond

By B. R. LAWN
H. H. Wills Physics Laboratory, University of Bristol
and H. KOMATSU
Royal Holloway College, Egham, Surrey

[Received 14 April 1966, and in revised form 26 May 1966]

ABSTRACT

The permanent surface distortions surrounding pressure crack figures on diamond surfaces have been studied by optical and x-ray topographic means. It is shown that the distortions are completely consistent with a permanent elastic deformation due to poor healing of the internal cracks. There appear to be no grounds for assuming that any micro-plastic flow has occurred.

§ 1. INTRODUCTION

IT was noted by Tolansky and Halperin (1954) that the octahedron faces of many natural diamonds are marked by numerous small polygonal crack figures. Subsequently, Howes and Tolansky (1955) succeeded in artificially producing similar figures, but on a larger scale, by statically loading diamond surfaces with a spherical indenter. From these studies it emerged that the crack figures on diamond are analogous to the familiar Hertzian ring cracks observed on similarly loaded glass surfaces.

The smooth pile-up of material surrounding a pressure crack has been interpreted in terms of two possible deformation mechanisms (Tolansky 1960). Firstly, the material may have undergone some micro-plastic flow. However, no trace of any slip lines has ever been detected in the piled-up region. Indeed, there is no conclusive evidence that plastic flow ever occurs in diamond below 1500°C (Evans and Wild 1965, 1966). The second possibility is that a permanent elastic deformation may be associated with the internal cracks. Although this mechanism has found relatively little favour in the literature it is deserving of a more detailed investigation as there is definite evidence that the crack interfaces do not 'heal' completely on removal of the load.

In this paper it is shown that the essential features of the surface distortion may be explained fully by a model based on the second of the mechanisms outlined above.

§ 2. AN ELASTIC DEFORMATION MODEL

Figure 1 (*a*) shows an idealized version of pressure crack formation in a brittle material. When the indenter load reaches a critical value the tensile stresses just outside the rim are sufficient to overcome the cohesive

strength of the material. A crack RLR′ then propagates as the load is increased. (If the load is increased still further multiple cracking may occur. We shall concern ourselves only with simple primary cracks.) In an elastically isotropic material such as glass the crack propagates down the 'Hertzian cone' of greatest tensile stress. In diamond the fracture tends to propagate more readily by easy cleavage along favourably oriented octahedral planes. This explains the tendency for pressure crack figures on diamond surfaces to be polygonal in shape. Upon release of the load (fig. 1 (*b*)) the material tends to return to its initial state but any 'debris' at the fracture interface will oppose complete recovery. When viewed optically the crack RLR′ appears to run back to a length RL′ but presumably the entire length RL remains effectively unhealed since the same cracks are easily made to reappear on reapplication of the load.

Fig. 1

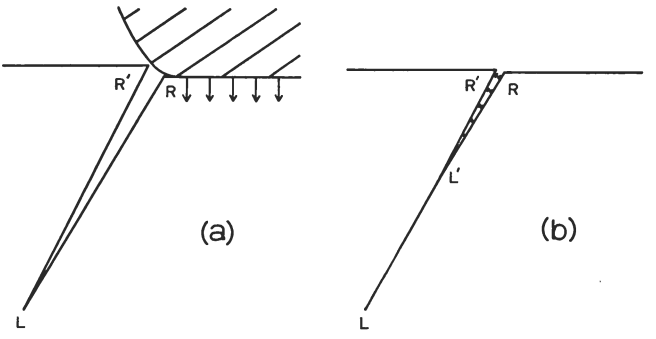

Formation of a pressure crack. (*a*) Under critical load, indenter induces crack RLR′. (*b*) On removal of indenter, crack appears to run back to RL′R′.

The residual deformation indicated in fig. 1 (*b*) now forms a convenient basis for establishing a workable elastic model. The deformation is taken to be equivalent to a distribution of normal stresses acting over both fracture surfaces. The nature of this distribution will not be very important since only the stresses acting near the mouth RR′ of the crack, where the bending moments are greatest and the dimensions of the material are least, will significantly distort the crystal. The straight edges of the crack figures then permit one to treat the material on either side of each edge as a long elastic wedge loaded along its tip R′ (or R) with a force **F** per unit length directed perpendicularly to the fracture interface. In fig. 2 R′ is the origin of coordinates (r, ϕ) with the sense of ϕ chosen so that $\phi = +\alpha$ at the crystal surface R′S and $\phi = -\alpha$ at the crack interface R′L. The stress distribution (Michell 1902) in such a loaded wedge is most conveniently obtained by assuming components $\mathbf{F}_0$ and $\mathbf{F}_{90}$ (fig. 2) of **F** to be applied

separately and by superposing solutions. This distribution is described completely by the radial stress:

$$\sigma_r = -\frac{F}{r}(K_0 \cos\phi + K_{90} \sin\phi),$$

where $K_0 = \sin\alpha/(\alpha + \frac{1}{2}\sin 2\alpha)$ and $K_{90} = \cos\alpha/(\alpha - \frac{1}{2}\sin 2\alpha)$. In an isotropic material the wedge angle 2α would be determined by the Hertzian cone angle. In diamond it is assumed to be determined by the orientation of favourable octahedral planes with respect to the crystal surface. (In the case of pressure cracks on octahedron surfaces the situation is not as simple as implied above and some non-crystalline fracture must occur. The reasons for this are simple crystallographic ones and are discussed fully by Howes (1965).)

From the stress-field the displacements $\mathbf{u}_r$ and $\mathbf{u}_\phi$ may be calculated. The following boundary conditions are assumed. By symmetry, at $\phi = 0$ and for all r, $u_\phi = 0$ with $\mathbf{F}_0$ acting and $u_r = 0$ with $\mathbf{F}_{90}$ acting. Also, at $\phi = -\alpha$ and $r = l$ (that is, at position L in fig. 2), $u_r = u_\phi = \partial u_\phi/\partial r = 0$.

Fig. 2.

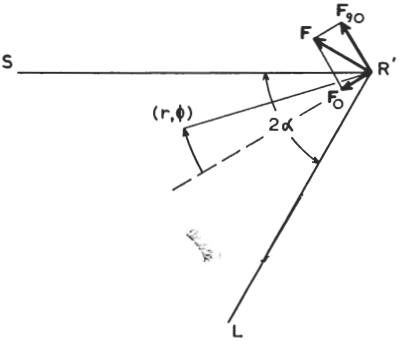

Crystal at piled-up edge of pressure crack treated as elastic wedge. For description, see text.

The quantity l should therefore give a measure of the unhealed crack length R'L. The magnitudes of $\mathbf{u}_r$ and $\mathbf{u}_\phi$ evaluated at the crystal surface ($\phi = \alpha$) are:

$$u_r = \frac{F}{E}(K_0 \cos\alpha + K_{90} \sin\alpha) \ln\frac{l}{r},$$

$$u_\phi = \frac{F}{E}\left\{(K_{90} \cos\alpha - K_0 \sin\alpha) \ln\frac{l}{r} + K_{90}\left(\frac{r}{l} - 1\right)\cos\alpha\right\}.$$

Young's Modulus E is taken to be 10^{13} dynes/cm^2. Owing to the assumption that $\mathbf{F}$ acts along a line instead of over a finite area the expressions imply infinite displacements at $r = 0$. The model is therefore unrealistic for small

regions near the wedge tips. Physically, these regions will extend from R′ (or R) down to the actual locations of the 'debris', a distance of the order of magnitude of several times the crack mouth separation RR′.

§ 3. Measurements of the Residual Deformation

3.1. *Optical Measurements of the Surface Profile*

Figure 3 shows two surface cracks, one on an octahedron and the other on a cube face, viewed in transmitted light. Both cracks were induced using a 0·7 mm diameter tungsten carbide ball as indenter. Prior to removal of the load the crack length RL was noted to be between 300 and 500 μm in each case. By way of comparison the optically visible crack RL′ is of the order of 100 μm in length. This latter segment of the internal crack is revealed on the micrographs as a complex pattern of ripple markings (attributable to interaction of the propagating crack with reflected stress waves) and cleavage steps. It is conceivable that these features are responsible for the poor healing of the internal cracks although one cannot discount the possibility that the indenter dislodges small fragments of material at R′ (fig. 1 (*a*)) and wedges them into the crack.

The diamond surfaces shown in fig. 3 have been surveyed by multiple beam interferometry. In particular the surface profiles along lines bisecting opposite sides of each crack figure have been accurately measured. It was found beneficial to use fairly broad fringes in order to smooth out irregularities due to natural damage on the octahedron surface and to polish-marks on the cube surface. The profile gives a measure of the displacement $\mathbf{u}_\phi$ evaluated at the crystal surface. From § 2 we see that the expression for this quantity contains both a logarithmic and a linear term in r. It may be shown that for typical values of α the linear term becomes important only when r exceeds about $l/3$. Thus for $r < l/3$ a plot of u_ϕ against $\ln r$ should give a straight line. Its slope $\partial u_\phi/\partial(\ln r)$ and intercept $\ln r_i$ extrapolated onto the abscissa axis are:

$$\frac{\partial u_\phi}{\partial(\ln r)} = -\frac{F}{E}(K_{90}\cos\alpha - K_0\sin\alpha),$$

$$\ln r_i = \ln l - \frac{K_{90}\cos\alpha}{K_{90}\cos\alpha - K_0\sin\alpha},$$

from which the parameters F and l may be evaluated.

For the piled-up regions of crystal such plots are shown in figs. 4 and 5. The hexagonal and square insets respectively refer to the two crack figures shown in figs. 3 (*a*) and (*b*). Note that there is no plot for edge 2 in fig. 4. Although it is not obvious from the micrograph in fig. 3 (*a*) this edge is multiply cracked. An examination of the diamond surfaces under a phase contrast microscope showed that the cracks at the edges of the square figure are also multiple ones, but not to the extent that the surface profile is noticeably disturbed. The graphs give reasonable straight lines which permit a straightforward evaluation of F and l (table). Variations in F reflect the degree of poor healing of the internal cracks. In particular,

Fig. 3

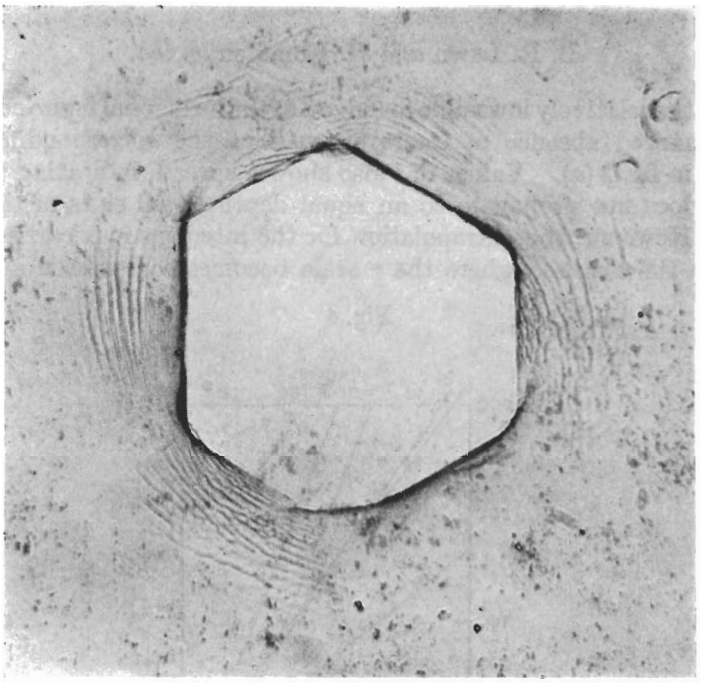

(*a*)

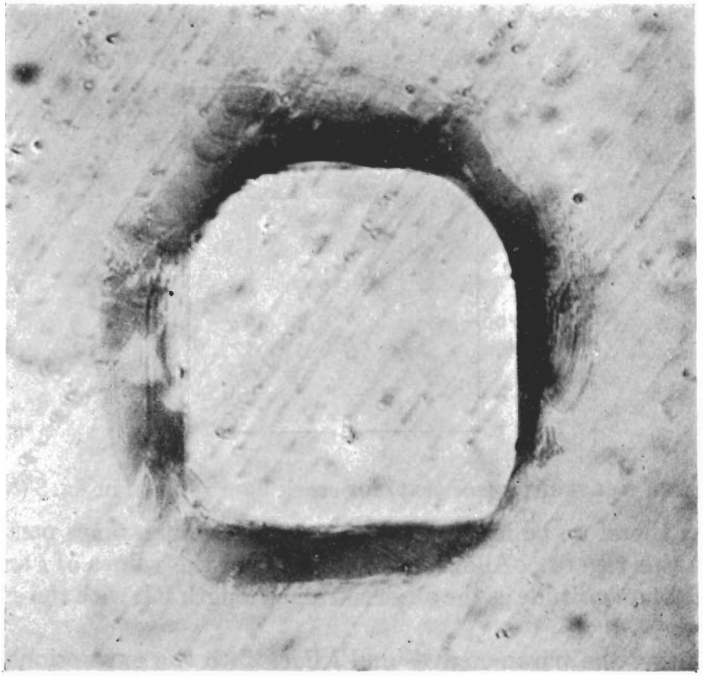

(*b*)

Pressure cracks on (*a*) natural octahedron, (*b*) polished cube face of diamond. Transmitted light. Note fracture detail (seen here out of focus) at internal crack interfaces. Diameter of cracks about 140 μm.

note that the relatively low value for edge 5 of the hexagonal figure correlates with a marked absence of fracture detail at the corresponding crack interface in fig. 3 (*a*). Values of l also show a spread, indicating that the fracture does not propagate to an equal depth on all sides of the crack figures. However, the extrapolation for the intercept r_i is carried into a region on the abscissa where the r scale becomes compressed and large

Fig. 4

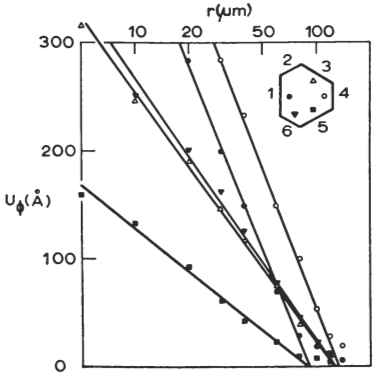

Plots of u_ϕ against r (see text) for crack figure shown in fig. 3 (*a*).

Fig. 5

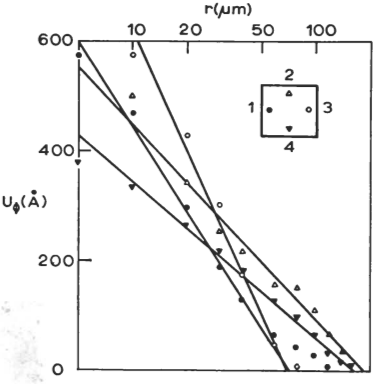

Plots of u_ϕ against r (see text) for crack figure shown in fig. 3 (*b*).

errors may therefore be incurred. Sides 1 and 3 in fig. 5 are particularly suspect in this regard. Allowing for this spread the values of l are of the same order of magnitude as the observed crack length RL with the specimen under load.

Substituting the parameters F and l back into the expressions for the displacements allows one to verify the approximation made by neglecting the linear term in r in the above analysis and also permits a computation of the surface profile of the central portion of the crack figure to be made.

Agreement between the computed profiles and those traced directly from Fizeau fringes is satisfactory (fig. 6). Note that the model predicts a small, flat depression of the central portion of the pressure crack. This feature is always observed in practice and has hitherto been regarded as strong evidence for the plastic flow mechanism.

Octahedron face

Side	F (10^5 dynes/cm)	l (μm)
1	42·8	265
2	—	—
3	22·7	373
4	44·1	385
5	13·7	248
6	25·4	356

Cube face

Side	F (10^5 dynes/cm)	l (μm)
1	20·1	199
2	13·4	513
3	27·7	194
4	10·9	452

Fig. 6

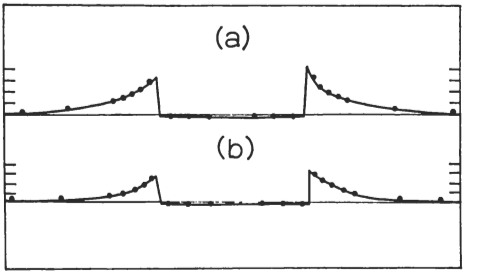

Measured (full line) and computed (black circles) surface profiles (*a*) along line bisecting sides 1 and 4 of figure on octahedron face and (*b*) along line bisecting sides 1 and 3 of the figure on cube face. Vertical scale divisions 100 Å in (*a*) and 200 Å in (*b*). Width of central portions on horizontal scale about 140 μm.

3.2. *X-ray Diffraction Topography*

An x-ray study of the pressure cracks discussed in the previous section has been made using transmission topography (Lang 1959) and reflection topography (Newkirk 1958). In order to be able to anticipate the nature of diffraction contrast if plastic flow indeed occurs around the cracks a comparative study was made of some Vickers pyramid indentations on an MgO crystal. The topographs of MgO revealed evidence for gross plastic deformation at the indentations. Traces of individual slip lines could also be clearly resolved in surrounding regions of crystal. No such trace of any dislocation mechanism could be detected on the topographs of the diamonds, the diffraction contrast being characteristic of a long-range elastic strain-field.

Transmission topographs of the diamonds are complicated by the fact that a projection of the entire crystal thickness is recorded on the photographic plate. In reflection topography, on the other hand, most of the intensity is diffracted from the first few extinction distances below the crystal surface. (One extinction distance using, say, the diamond 004 Bragg-case reflection with CuKα radiation, is 3μm.) Consequently we will discuss only the reflection topographs with their simpler diffraction geometry. Two examples are shown in fig. 7, the outlines of the crack figures (with the same orientations as in fig. 3) being faintly visible in each case. (Note that some of the more severe abrasion tracks on the cube surface (fig. 7 (*b*)) also show diffraction contrast. Since the surface damage sustained by diamond during abrasion has been likened to partial pressure crack formation (Seal 1958) it is probable that this contrast is due to the same form of strain-field as exists around a single pressure crack.) The diffraction contrast mechanism causing the intense 'halos' is not well understood. Since the incident x-ray beam used in these experiments has an angular divergence considerably greater than the total range of reflection of the perfect crystal some form of 'extinction contrast' occurs when the elastic distortion exceeds a certain magnitude (Webb 1962). That the image blackening does not extend up to the sides of the crack figures is due to crystal near the crack edges being elastically distorted to the extent that the Bragg condition is no longer satisfied locally. This has been verified by increasing the angular divergence of the incident beam still further. Topographs of the faces taken with this modified arrangment showed considerable extension of image blackening towards the crack edges. By increasing the divergence the more distorted regions of crystal have been brought into a reflecting position.

§ 4. Conclusion

The foregoing sections show that the surface distortion about a pressure crack on diamond is consistent with the proposed elastic model. No evidence has been found, either optically or topographically, to suggest that any micro-plastic flow occurs. The elastic deformation mechanism

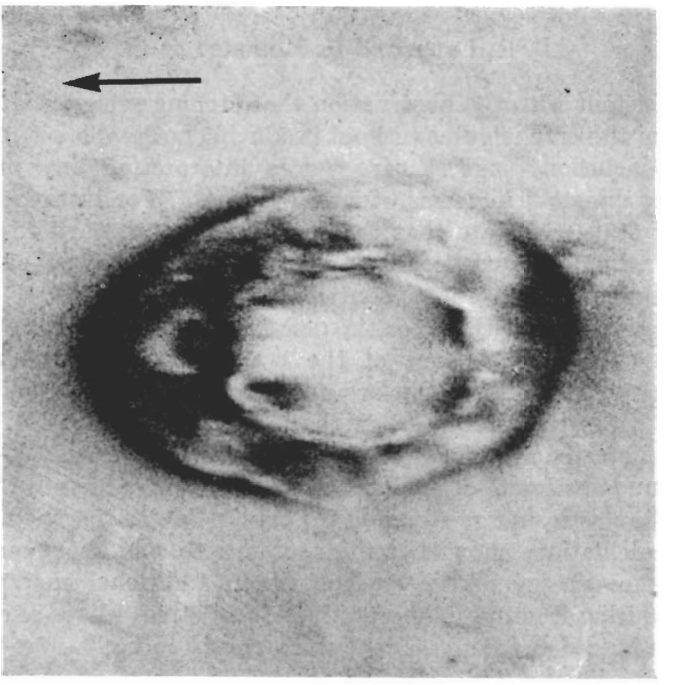

(*a*)

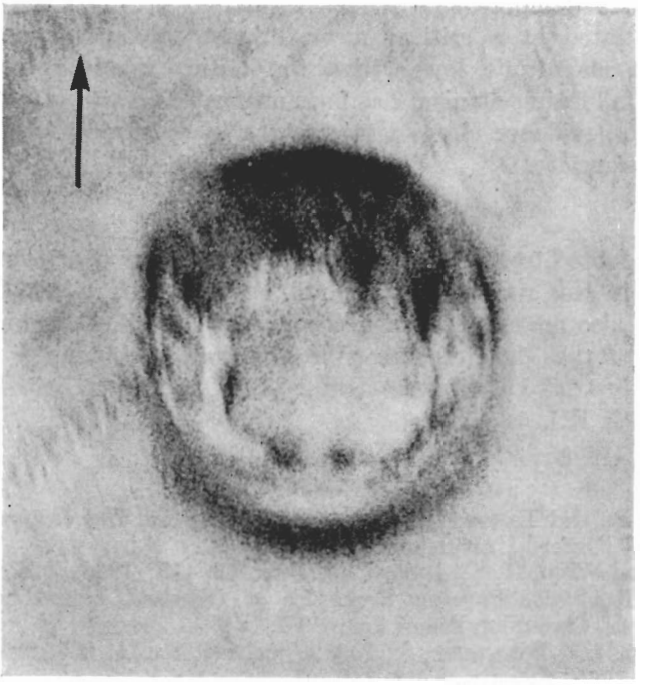

(*b*)

X-ray reflection topographs, (*a*) (111) surface, 220 reflection, CrKα radiation, (*b*) (001) surface. 004 reflection, CuKα radiation. Arrows are projections of reciprocal lattice vectors on to image planes.

is also consistent with the observation that etching preferentially attacks the edges of the crack figures without producing noticeable pitting nearby.

These conclusions suggest care before interpreting any mechanical property of diamond in terms of a slip process. For instance, Bowden and Tabor (1964) indicate that the surface energy of partial ring cracks formed on a diamond surface, across which a diamond stylus (load ~ 1 Kg) has been dragged (Seal 1958), contributes only about 1% to the total frictional energy and that plastic deformation may account for the remainder. The surface area of the crack interface is estimated by polishing away the diamond surface until the cracks are no longer visible optically. However, it is possible that only the portions RL'R' of the cracks are detected in this way. As indicated in § 3.1 this could result in a gross underestimate of the surface area. To be added to the surface energy is the elastic energy stored in the crystal due to the residual strain, although calculations show that this amounts to only about ten per cent of the surface energy of the cracks. Much additional energy is often expended during fracture in the production of stress waves and cleavage steps, as is indeed suggested by the micrographs in fig. 3.

Other experiments have also led to the conjecture of possible plastic flow in diamond at room temperature. (For a summary see Bowden and Tabor 1964). A deformation similar to that observed about a statically induced pressure crack is observed when a diamond surface is repeatedly impacted with a diamond ball. After several thousand impacts a percussion crack is initiated at a critical mean impact pressure approximately an order of magnitude lower than the critical static pressure. The cumulative failure mechanism has been suggested as one of plastic flow: in view of the evidence above a microcrack mechanism would appear to be more appropriate.

Acknowledgments

We are indebted to Professor F. C. Frank for many discussions and for his interest in this work. Professor S. Tolansky, Dr. A. R. Lang and Dr. M. Hart also made useful suggestions. Mr. A. Duckett prepared the topographs of the MgO crystal. We acknowledge financial assistance from an Industrial Distributors Grant (B.R.L.) and a British Council Scholarship (H.K.).

References

Bowden, F. P., and Tabor, D., 1964, *The Friction and Lubrication of Solids*, Part II (Oxford University Press), Chap. X.

Evans, T., and Wild, R. K., 1965, *Phil. Mag.*, **12**, 479; 1966, *Ibid.*, **13**, 209.

Howes, V. R., 1965, *Physical Properties of Diamond*, edited by Berman (Oxford: Clarendon Press), Chap. VI.

Howes, V. R., and Tolansky, S., 1955, *Proc. roy. Soc.* A, **230**, 287, 294.

Lang, A. R., 1959, *Acta Cryst.*, **12**, 249.

Michell, J. H., 1902, *Proc. Lond. math. Soc.*, **34**, 134.

Newkirk, J. B., 1958, *Trans. A.I.M.E.*, **215**, 483.

SEAL, M., 1958, *Proc. roy. Soc.* A, **248,** 379.
TOLANSKY, S., 1960, *Surface Microtopography* (London: Longmans, Green & Co.), Chap. XIX.
TOLANSKY, S., and HALPERIN, A., 1954, *Proc. phys. Soc. Lond.*, B, **67,** 473.
WEBB, W. W., 1962, *Direct Observations of Imperfections in Crystals*, edited by J. B. Newkirk and J. H. Wernick (New York: Interscience), p. 62.